PCCP

Electrochemistry of Layered GaSe and GeS: Applications to ORR, OER and HER

Journal:	*Physical Chemistry Chemical Physics*
Manuscript ID	CP-ART-11-2015-006682.R1
Article Type:	Paper
Date Submitted by the Author:	24-Nov-2015

Complete List of Authors:	Tan, Shu Min; Nanyang Technological University, Division of Chemistry and Biological Chemistry Chua, Chun Kiang; Nanyang Technological University, Chemistry and Biological Chemistry Sedmidubsky, David; Institute of Chemical Technology, Sofer, Zdenek; Institute of Chemical Technology, Prague, Department of Inorganic Chemistry Pumera, Martin; Nanyang Technological University, Chemistry and Biological Chemistry

Electrochemistry of Layered GaSe and GeS: Applications to ORR, OER and HER

Shu Min Tan,[a,‡] Chun Kiang Chua,[a,‡] David Sedmidubský[b], Zdeněk Sofer[b] and Martin Pumera[a]*

[a] School of Physical and Mathematical Science, Division of Chemistry and Biological Chemistry, Nanyang Technological University, 21 Nanyang Link, Singapore 637371.

[b] Department of Inorganic Chemistry, University of Chemistry and Technology Prague, Technická 5, 166 28 Prague 6, Czech Republic.

Keywords: Gallium selenide, germanium sulfide, electrochemistry, layered materials, hydrogen evolution reaction.

ABSTRACT: Though many studies examined the properties of the class of IIIA-VIA and IVA-VIA layered materials, few have delved into the electrochemical aspect of such materials. In light of the burgeoning interest in layered structures towards various electrocatalytic applications, we endeavored to study the inherent electrochemical properties of representative layered materials of this class, GaSe and GeS, and their impact towards electrochemical sensing of redox probes as well as catalysis of oxygen reduction, oxygen evolution and hydrogen evolution reactions. Contrary to the typical sandwich structure of MoS_2 layered materials, GeS is isoelectronic to black phosphorus with the same structure; GaSe is a layered material consisting of GaSe sheets bonded in the sequence Se–Ga–Ga–Se. We characterized GaSe and GeS by employing scanning electron microscopy, X-ray diffraction, Raman spectroscopy and X-ray photoelectron spectroscopy complemented by electronic structure calculations. It was found that the encompassing surface oxide layers on GaSe and GeS greatly influenced their electrochemical properties, especially their electrocatalytic capabilities towards hydrogen evolution reaction. These findings provide fresh insight into the electrochemical properties of these IIIA-VIA and IVA-VIA layered structures which enables development for future applications.

Introduction

The class of IIIA-VIA and IVA-VIA layered semiconductors presents a group of largely layered two-dimensional materials. These layered materials generally possess the chemical formula MX, where M = Ga/In (Group IIIA) or Ge/Sn (Group IVA) and X = S/Se/Te (Group VIA), but other chemical formulae exist as well.[1,2] Gallium selenide and germanium sulfide layered materials are structurally similar to transition metal dichalcogenides (TMDs) and black phosphorus respectively, with strong in-plane covalent bonding and weak out-of-plane van der Waals interactions.[3-6] GaSe and GeS are two representative compounds of the family of IIIA-VIA and IVA-VIA layered materials. The GaSe crystal displays a layered hexagonal structure (space group P-6m2), in which each layer consists of GaSe sheets bonded in the sequence Se–Ga–Ga–Se; each Ga atom is tetragonally bonded to one Ga atom and three Se atoms, while each Se atom is trigonally bonded to three Ga atoms.[7] On the other hand, GeS exhibits an orthorhombic structure (space group Pnma), whereby each layer consists of the sequence Ge–S–Ge–S and each Ge atom is bonded to three Se atoms and vice versa.[8] This structure is similar to black phosphorus, which is isoelectronic with GeS (see Figure S2 for schematic representations of GaSe and GeS). In contrary to black phosphorus, which is very sensitive towards water vapor, GeS is highly stable at ambient conditions.[9,10] Similarly to black phosphorus, GeS exhibits low toxicity.[11] As a result of their optical and electronic attributes, coupled with semiconducting properties which are similar to those of Group VIB-VIA TMDs such as MoS_2 and WS_2, they are often explored for use as electrical sensors, and photoelectric and nonlinear optical devices.[12-14] Over the last few decades, much progress has been made in the synthesis of such materials, leading to the development of methods such as chemical vapor deposition (CVD) using various precursors,[8,13] the Bridgman method,[15-17] plasma discharge of precursors,[18] electrodeposition[19] and chemical reduction[20] for the fabrication of IIIA-VIA and IVA-VIA layered semiconductors.

In recent years, investigations into the properties of such layered materials (e.g. GaS, SnS, InSe and InTe) have been conducted.[21-27] However, the fundamental electrochemical properties of the IIIA-VIA and IVA-VIA layered materials remain predominantly unexplored. Of late, it has been reported that some of these IIIA-VIA and IVA-VIA layered materials show promising results as anodes in lithium-ion batteries, amongst other energy-related electrochemical applications such as hydrogen evolution reaction (HER).[20,25,28] Hence it is imperative to examine the electrochemical properties of these layered materials, both inherent and with respect to potential alternative energy-related electrochemical applications e.g. HER, oxygen evolution reaction (OER) and oxygen reduction reaction (ORR).

Herein, we have synthesized and characterized both GaSe and GeS using scanning electron microscopy (SEM), energy-dispersive X-ray spectroscopy (EDS), X-ray diffraction (XRD), Raman spectroscopy and X-ray photoelectron spectroscopy (XPS), complemented by electronic structure calculations and photoluminescence measurements. We will be examining their inherent electrochemistry, together with evaluations of their intrinsic heterogeneous electron transfer using $Fe(CN)_6^{3-/4-}$ and $Ru(NH_3)_6^{3+/2+}$ redox probes. Studies on their electrocatalytic activities towards the three electrochemical reactions, HER, OER and ORR, which serve as potential alternative sources of energy, will be discussed in detail as well.

Results and Discussion

In this study, we examined the electrochemical properties of IIIA-VIA and IVA-VIA layered materials by employing GaSe and GeS as typical representatives of this class of materials. Besides investigating into their inherent electroactivities and heterogeneous electron transfer rates, we will also be assessing their electrocatalytic capabilities towards HER, OER and ORR. This first in-depth investigative study on the electrochemical properties of IIIA-VIA and IVA-VIA layered materials will drive the development of such materials for various electrochemical applications.

Electronic structure determination of GaSe and GeS

The semiconducting nature of GaSe and GeS is well-studied in the field of optoelectronics. However, associations between their electronic structures and electrochemical properties are obscure. Here, we examined the electronic properties of GaSe and GeS via both DFT calculations and photoluminescence measurements, as a more fundamental approach to understanding their electrochemical characteristics.

Considering the structure analogy between black phosphorus and GeS, it is not surprising that its band structure (Figure 1A) reveals several similarities. Much like in black phosphorus, the valence states are spread down to ~15 eV below the Fermi level and are separated by a band gap 1 eV (1.25 eV for a single layer) from the conduction band of primarily Ge 4p character. However, compared to black-P, the band gap is larger and indirect. Moreover, due to a slight difference in electronegativity between Ge and S, we can distinguish the S 3s band located at 12.5–14.5 below E_F and the large valence band of ~5 eV with predominant S 3p character. Between these two bands, a Ge 4s band can be clearly identified corresponding to Ge(II) valence state. The single layer calculation yielded the work function 4.57 eV; cf. with 4.92 eV for black-P.

The main features on the density of states (DOS) calculated for GaSe (right panel in Figure 1B) are similar to that of GeS, with an additional narrow band around 15 eV below E_F formed by Ga 3d states. The direct band gap of 1 eV (at Γ-point) is apparently underestimated compared to the experimental value obtained from photoluminescence (to be discussed later), but agrees with previous calculations.[29-31] Nevertheless, the main difference between the two chalcogenides can be seen in the unusual valence state of Ga(II) which is established as a result of direct Ga-Ga bonding. This brings about a splitting of Ga 4s states leaving two bands ~7 eV below E_F and the other two empty bands at the lower edge of the conduction band, whereas all Ge 4s bands in GeS are well below E_F.

The total energies resulting from the calculation of bulk structures were referred to the energies of the corresponding elements in their standard forms stable at room temperature (Ga, Ge, S, Se) yielding the enthalpies of formation at T = 0 K, $\Delta_f H_0$(GeS) = –57.9 kJ mol^{-1} and $\Delta_f H_0$(GaSe) = –113.7 kJ mol^{-1}. The value obtained for GeS is in very good agreement with the assessed value $\Delta_f H_{298}$(GeS) = –61.2 kJ mol^{-1}.[32] However, the calorimetry and vapor pressure values reported for GaSe ($\Delta_f H_{298}$(GaSe) = –146.4±12.6 kJ mol^{-1} and –157.7±0.9 kJ mol^{-1})[33,34] are much more exothermic and, thus, the differences between the experimental and calculated values can hardly be accounted for just by the integral of ΔC_p from 0 K to 298 K. With consideration of the spin-orbit interaction, particularly for Se, the structure is stabilized by –2 kJ mol^{-1}, which is insufficient to account for the large differences. Surprisingly, calculations of the energy of GaSe for its second reported structure arrangement ($P6_3mmc$ space group), differing only in the stacking pattern of individual layers (simple –ABABAB-pattern compared to -ABCBAB- pattern present in P-6m2), yielded an even less exothermic value of $\Delta_f H_0$(GaSe) = –85.6 kJ mol^{-1}, which is very similar to that of the monolayer (–82.4 kJ mol^{-1}). The bulk structure is thus stabilized by a relatively strong interlayer coupling also manifested by a fairly large surface energy γ(GaSe) = 383 mJ m^{-2}; cf. with γ(GeS) = 67 mJ m^{-2}. This contradicts the highly anisotropic lamellar character of GaSe microstructure which cannot be removed even after long term milling and precludes an accurate structure determination from powder XRD. We can thus surmise a more complex stacking pattern present in the powder material, stabilizing the structure compared to the P-6m2 arrangement considered in our calculations.

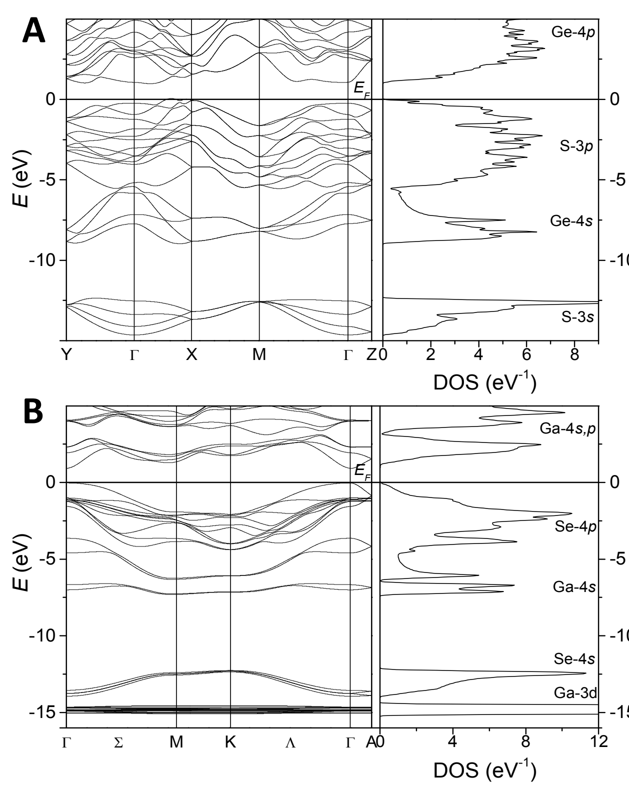

Figure 1. Band structure along the principle directions of the first Brillouin zone (left) and the corresponding density of states (DOS) (right), plotted for (**A**) GeS and (**B**) GaSe.

To experimentally investigate band gaps of the synthesized materials, photoluminescence measurements were performed and the spectra are given in Figure S3 (ESI). GaSe exhibits a strong narrow luminescence, characteristic of a direct band gap semiconductor, with maxima at 621 nm corresponding to 1.996 eV. On the other hand, GeS is an indirect band gap semiconductor and demonstrates significantly weaker luminescence signal with a maxima at 753 nm, corresponding to 1.647 eV. Though both materials afforded experimental values that are lower than those calculated by DFT, they are consistent with the values reported in literature.[35,36]

Characterizations of GaSe and GeS

In order to examine any structural differences between the two layered materials after the fabrication process, SEM was employed to investigate the surface morphologies of GaSe and GeS powders used for electrochemical characterizations. Figure 2 displays the scanning electron micrographs of GaSe and GeS, taken at 10 000× magnification. The layered structures were clearly discerned, as indicated by the white arrows in the micrographs. These structures appear to be stacked, implying a bulk assembly of layers with several cracks between individual layers. This originates from intensive mechanical disintegration by long term mechanical agitation in agate mortar. Further elemental analyses and chemical characterizations of the bulk GaSe and GeS were performed using EDS, with homogeneous distributions of Ga, Se, Ge and S apparent from the elemental mappings, as displayed in Figure S1 (ESI). The M:X ratios obtained from EDS analyses are slightly enriched with metal atoms, and are different from those acquired from XPS (to be discussed later). This is attributed to differences in the depth and area of analysis of the two techniques, as well as their relative sensitivity to various elements. Overall, SEM demonstrated the morphologies of GaSe and GeS which are characteristic of bulk layered materials, while EDS provided bulk analyses of their elemental compositions and distributions.

Subsequently, Raman spectroscopy was exploited to examine the vibration modes of GaSe and GeS as verifications of their layered structural compositions. Figure 3 exhibits the Raman spectra of both GaSe and GeS. From the Raman spectrum of GaSe (Figure 3A), four distinct peaks were observed: two out-of-plane vibration modes A^1_{1g} and A^2_{1g} at ca. 122 and 297 cm^{-1} respectively, one in-plane E_{2g} at ca. 201 cm^{-1}, and one in-plane vibration mode E_{1g} at ca. 240 cm^{-1} (denoted based on D_{6h} point group).[37] There is a consistent red shift of ca. 10 cm^{-1} in the peak values of all four vibration modes cf. literature values,[37] which may be due to thermal expansion of the crystals during the measurements.[38] The presence of these characteristic peaks indicates a layered structure for GaSe, with individual layer containing four sheets of atoms bonded in the *c*-direction, in sequence of Se–Ga–Ga–Se.[38]

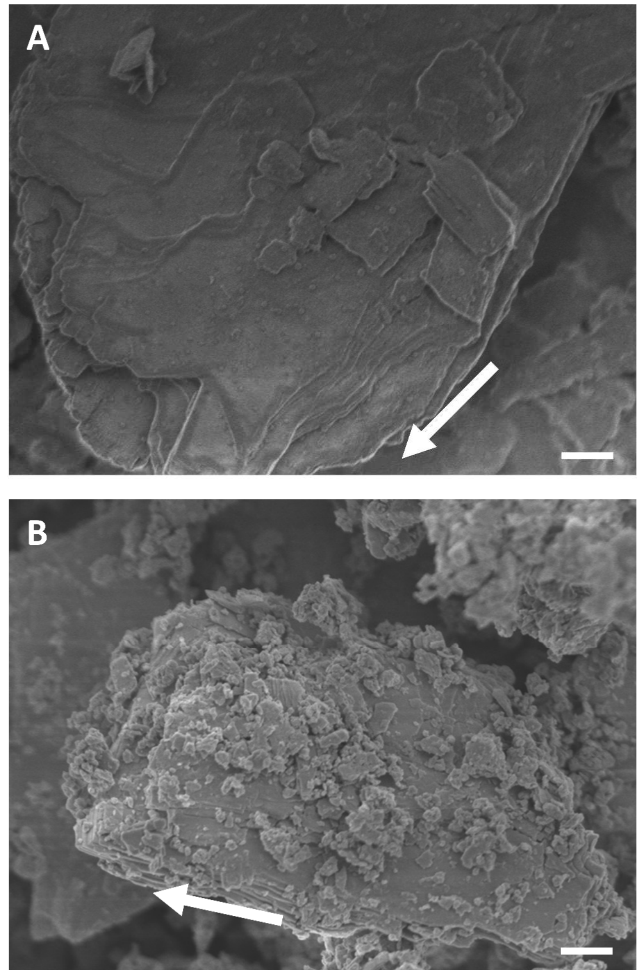

Figure 2. Scanning electron microscopy (SEM) images of (**A**) GaSe and (**B**) GeS displaying the layered structures of the materials (directions of the basal planes are indicated by the arrows) at 10 000× magnification. Scale bars represent 1 μm.

On the other hand, from Figure 3B, the Raman peaks for GeS were not as well-defined as those for GaSe. Three broad peaks were identified: one in-plane shearing mode B_{3g} at ca. 194 cm^{-1}, one out-of-plane compressive mode B_{2g} at ca. 223 cm^{-1} (overlapped with the in-plane A_{1g} mode), together with one in-plane shearing mode A_{1g} at ca. 253 cm^{-1} (denoted based on D_{2h} point group).[39] Similar to the case of GaSe, the peak values are red shifted cf. literature values.[39,40] Here, the more probable cause may be due to the composition of GeS within the crystal. It has been reported that sulfur-enriched GeS ($Ge_{40}S_{60}$) exhibits a large broad peak in place of the three identified in this paper, with peak width of ca. 100 cm^{-1}, as a result of disrupted layered structure.[41] This suggests that the GeS synthesized here is enriched with sulfur which is substantiated with X-ray photoelectron spectroscopy (XPS) data in the ensuing paragraphs. XRD was also performed to examine the phase purity of the synthesized materials. The X-ray diffractograms (Figure S2 in ESI) demonstrated the phase purity of GaSe and GeS, corresponding to hexagonal GaSe and orthorhombic GeS. These results, together with the Raman spectra, reveal the layered structure of GaSe and GeS phases, indicating successful fabrication of these layered materials and allowing for further characterization.

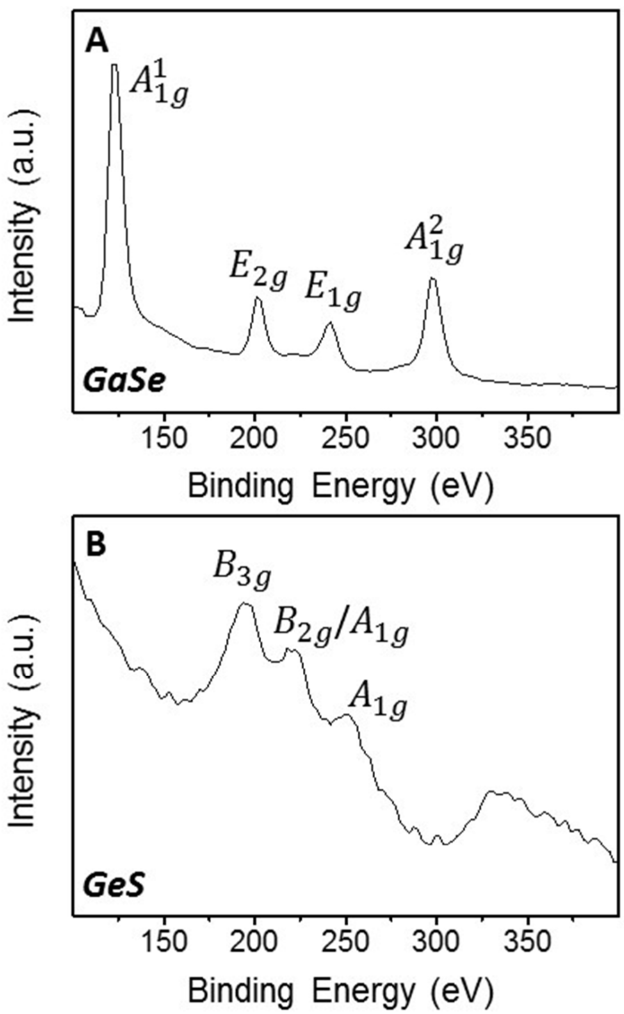

Figure 3. Raman spectra of (**A**) GaSe and (**B**) GeS. λ_{ex} = 514.5 nm.

While both XRD and Raman provide structural information on GaSe and GeS, they do not shed light on the chemical compositions of the materials. Hence, XPS was performed to examine the surface chemical compositions of GaSe and GeS. Figure 4 exhibits the wide scan XPS spectra of GaSe and GeS, together with their electrochemically pre-treated counterparts. These materials display inherent electrochemistry (to be discussed later), which we postulate to have an impact on their electrochemical properties, hence surface chemical composition analyses were performed on both electrochemically oxidized and reduced GaSe and GeS (see Experimental for pre-treatment conditions). The wide scan spectra indicate the presence of gallium and selenium in GaSe and germanium and sulfur in GeS; oxygen and carbon are present in both materials, the latter of which is attributed to adventitious carbon species[42] and the C 1s peak was used for calibration at 284.5 eV. These wide scan spectra provide limited information on the elements present on the surface of GaSe and GeS, hence the high resolution XPS core-level spectra of various elements were examined, as illustrated in Figure 5. The atomic percentages of Ga 3d, Se 3d, Ge 3d, S 2p, O 1s and C 1s peaks, along with the M:X ratios, are presented in Table 1. A crucial observation derived from the M:X ratios is that none of the materials exhibit a ratio of 1, as expected from the chemical formula of these IIIA-VIA and IVA-VIA materials. This suggests more complex surface chemical compositions of GaSe and GeS than that initially contemplated.

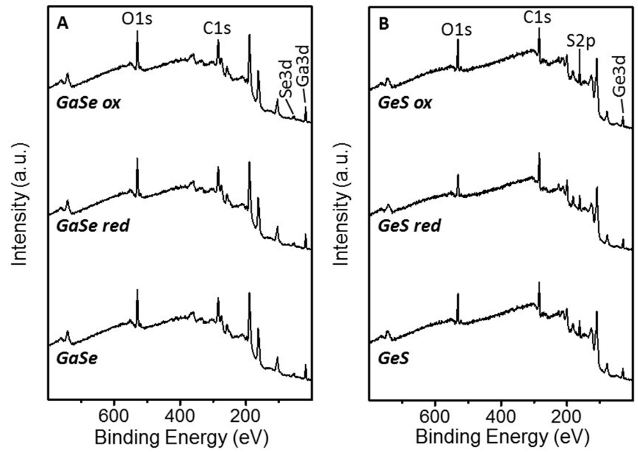

Figure 4. Wide scan X-ray photoelectron spectra (XPS) of (**A**) GaSe and (**B**) GeS. Calibration was performed using the adventitious C 1s peak, referenced at 284.5 eV.

Figure 5A and C show the deconvolution of the core-level Ga 3d and Ge 3d spectra into two pairs of peaks; one pair corresponds to Ga-Se and Ge-S bonds (at ca. 19.6 and 20.0 eV and ca. 30.3 and 30.9 eV respectively),[43,44] and the other originates from the respective oxidation states of metal oxides (at ca. 20.1 and 20.6 eV and ca. 32.2 and 32.8 eV correspondingly).[43,45] This is likely due to the surface oxidation related to the relatively low stabilities of Ga^{2+} and Ge^{2+}; the covalent character of metal-chalcogen bonds together with low oxidation state of the metal led to the easy surface oxidation and formation of gallium(III) and germanium(IV) oxide respectively. For GaSe, the oxides originate from a layer of gallium oxide i.e. Ga_2O_3, which is insoluble in aqueous solution,[46,47] passivating the GaSe surface and preventing the underlying material from further oxidation.[48] Upon closer inspection of the M:X ratios of GaSe in Table 1, it is interesting to note that all examined materials are chalcogen-deficient, whereby the M:X ratio decreases from 7.12 in the untreated GaSe to 1.36 in the reduced GaSe, and to 6.55 in the oxidized equivalent. The passivating Ga_2O_3 layer envelopes the untreated GaSe, resulting in much higher M:X ratio than expected. From the untreated GaSe to the reduced counterpart, the decrease in M:X ratio, albeit to non-unity, denotes the partial removal of surface oxides, possibly to soluble products such as GaO_2^- in alkaline environment or Ga^{3+} in acidic enviroment.[48] On the other hand, a reduction in M:X ratio in the oxidized GaSe indicates that some of the surface oxides may have been converted to aqueous species such as Ga^{3+},[48] resulting in lower atomic percentage of Ga 3d after oxidation.

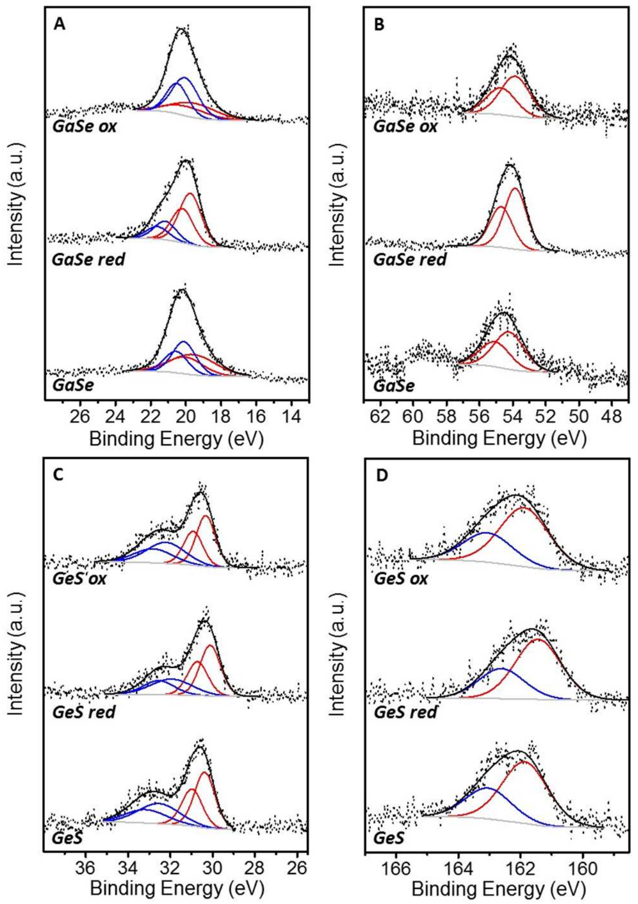

Figure 5. High resolution XPS core-level (**A**) Ga 3d and (**B**) Se 3d spectra of GaSe, and high resolution XPS core-level (**C**) Ge 3d and (**D**) S 2p spectra of GeS. Each pair of fitted peaks with matching color corresponds to the respective spin-orbit coupled peaks. Calibration was performed using the core-level C 1s peak, referenced at 284.5 eV.

For GeS, the M:X ratios for the untreated, electrochemically reduced and oxidized materials exhibit a trend opposite to that observed for GaSe: all the materials are chalcogen-enriched. However, as aforementioned, the GeS surface is covered with an abundant of metal oxides (Figure 5C), likely to be GeO_2 (ca. 32.2 and 32.8 eV),[45] in which case there should be a deficit of sulfur atoms. Hence, it is probable that the chemical composition of the GeS surface is of the form GeS_x, $1 < x < 2$, corroborating the Raman spectroscopy results. As such, the GeS materials are, in fact, chalcogen-deficient. Both electrochemical pre-treatments of GeS resulted in lower M:X ratios (0.73 and 0.69 for reduced and oxidized GeS respectively), indicating increases in relative sulfur content on the surface of GeS. The decrease in M:X ratio after electrochemical reduction resulted from partial removal of GeO_2, as well as dissolution of GeO_2.[49,50] Simultaneously, part of the oxidized Ge^{4+} may form GeS_2 on the surface with M:X ratio equal to 0.5. On the other hand, electrochemical oxidation accelerated the formation of GeO_2 on the surface of GeS, which subsequently underwent dissolution in water, resulting in lower M:X ratio.

On the whole, from all the performed characterizations, it was gathered that the fabricated GaSe and GeS were layered structures, covered with a significant amount of metal oxides on the surface. In particular, GeS is sulfur-enriched, and is likely to contain GeS_2 on the surface. Hereafter, equipped with these information, we proceeded to study the electrochemical properties of these materials.

Inherent electrochemistry of GaSe and GeS

The electrochemical window of materials is governed by their inherent electroactivity, which stems from redox-active components on the surface, or electrochemical decomposition of the solvent.[51,52] Besides TMDs and graphene oxides,[53-55] a plethora of layered structures such as layered transition metal oxyhydroxides and layered black phosphorus, among others,[6,56-59] have shown inherent electrochemical activities that restrict their operating potential windows and interfere with the sensing of common redox probes and important analytes such as pesticides and mycotoxins.[52,60] Moreover, the emerging application of IIIA-VIA and IVA-VIA materials for various electrocatalytic functions[20,25,28] renders it imperative to investigate the inherent electrochemical behaviors of GaSe and GeS as representatives of this class of materials. With this aim in mind, we performed an examination of the intrinsic electroactivities of GaSe and GeS by employing cyclic voltammetry (CV).

The inherent electrochemical performances of GaSe and GeS, which was investigated over the range of ±1.5 V in nitrogen-purged phosphate buffer solution (PBS, pH 7.2), are illustrated in Figure 6. GaSe exhibits a small anodic current from ca. +0.5 V to +1.0 V for both anodic and cathodic initial scan directions, and no inherent reduction peak was observed. It is clear that GaSe undergoes oxidation, possibly to Ga_2O_3,[48] and subsequent passivation by the oxide layer prohibits further electrochemical response of the material. In comparison to GaSe, GeS displays a much smaller operating potential window, due to the presence of a broad inherent oxidation peak from ca. +0.5 V to +1.3 V and a small reduction peak at ca. –1.0 V (Figure 6C). When the scan direction was reversed, no inherent reduction peak was detected in the first cycle, while the observed reduction peak appeared only after the occurrence of the inherent oxidation peak of GeS. This suggests that the two redox peaks arise from the same electrochemical process, which was ascribed to the redox of the $Ge^{2+/4+}$ species, with GeS in the reduced state initially. It is probable that upon oxidation, Ge^{4+} forms GeO_2 which subsequently undergo dissolution, hence a decreasing trend with every cycle is observed for the inherent oxidation peak.

Table 1. Atomic percentages of various elements present in GaSe and GeS, before and after electrochemical reduction and oxidation, together with the metal:chalcogen (M:X) ratio of each material.

Material[a]	Ga 3d (at.%)	Se 3d (at.%)	Ge 3d (at.%)	S 2p (at.%)	O 1s (at.%)	C 1s (at.%)	M:X ratio
GaSe-unt	12.5	1.8	-	-	30.8	55.0	7.12
GaSe-red	11.8	8.6	-	-	19.3	60.2	1.36
GaSe-ox	12.3	1.9	-	-	34.6	51.2	6.55
GeS-unt	-	-	8.0	10.0	23.5	58.6	0.80
GeS-red	-	-	8.1	11.1	24.2	56.6	0.73
GeS-ox	-	-	8.3	11.9	26.4	53.4	0.69

[a]GaSe-unt, GaSe-red and GaSe-ox denote untreated GaSe, electrochemically reduced GaSe, and electrochemically oxidized GaSe respectively. Similar notations apply to the GeS materials as well.

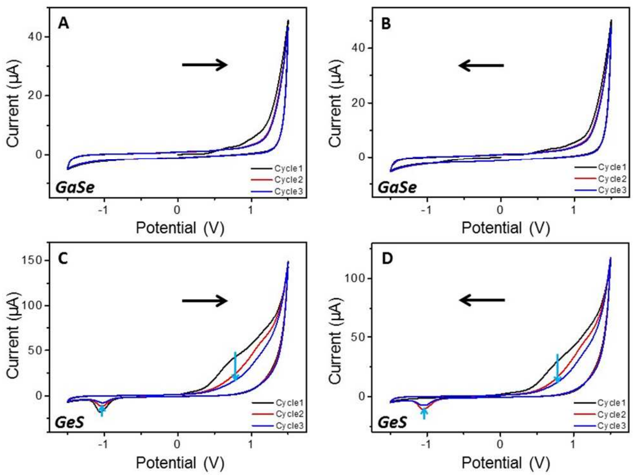

Figure 6. Cyclic voltammograms of the inherent electrochemical performances of (**A** and **B**) GaSe and (**C** and **D**) GeS. Three consecutive cycles of CV were performed and all CVs commence from 0 V, with the black arrows indicating initial scan direction. Conditions: scan rate of 100 mV s^{-1}, 50 mM PBS (pH 7.2) as supporting electrolyte.

From the inherent electrochemical study of GaSe and GeS, the following conclusions can be drawn: (1) GeS exhibits a smaller operating potential window, centered mainly in the cathodic region, while GaSe demonstrates a wide potential window, suitable for studying a broad range of electrochemical reactions. (2) GaSe surface is passivated towards inherent oxidation/reduction upon the second cycle, while GeS remains electroactive throughout the measurement albeit with decreasing activity. These suggest possible interference in the sensing of redox probes and their electrocatalytic capabilities towards various reactions which we subsequently endeavor to investigate.

Electrochemical sensing by GaSe and GeS

Typically, a preliminary study to examine the suitability of an electrode material for electrochemical sensing is the measurement of its observed heterogeneous electron transfer (HET) rate, whereby an innately rapid HET rate implies lower overpotential for the occurrence of an electrochemical reaction. In the following study, we investigated the HET rates of GaSe and GeS through CV measurements of $Fe(CN)_6^{3-/4-}$ and $Ru(NH_3)_6^{3+/2+}$ redox probes, which are commonly used for electrochemical sensing purposes. The peak-to-peak separation (ΔE) of the voltammograms can be related to the HET rate constant, k^0_{obs}, through the Nicholson method,[61] whereby wider separation between the redox peaks corresponds to slower HET and smaller k^0_{obs}.

The $Ru(NH_3)_6^{3+/2+}$ redox probe typically exhibits a pair of redox peaks over the range from –1.0 V to +0.6 V which is the region in between the two redox peaks observed for GeS (Figure 6C and D). Moreover, $Ru(NH_3)_6^{3+/2+}$ is an outer-sphere probe which is dependent on DOS but is insensitive to surface microstructures and oxides of electrode materials; its electrochemical signal should be independent of any interaction with the electrode surface.[62] Hence, the exploitation of this redox probe will allow us to determine the feasibility of GaSe and GeS in sensing applications. Figure 7A shows the cyclic voltammograms of $Ru(NH_3)_6^{3+/2+}$ on bare glassy carbon (GC) electrode, GaSe and GeS. All three electrode materials attained similar ΔE (difference in ΔE = ca. 3 mV) with comparable peak heights: k^0_{obs} of the bare GC electrode, GaSe and GeS were calculated to be 4.5 × 10^{-3} cm s^{-1}, 4.4 × 10^{-3} cm s^{-1} and 4.3 × 10^{-3} cm s^{-1} respectively. This is consistent with the DFT calculations whereby both GaSe and GeS exhibit similar DOS at E_F. In particular, the asymmetric voltammogram of GeS stems from the inherent electrochemistry of GeS, where the initial arc of the inherent oxidation peak can be seen in the anodic potential region. The onset of GeS reduction in the cathodic end of the potential range was observed as well. However, despite these, the k^0_{obs} derived from GeS remained close to that of bare GC.

The CV of $Fe(CN)_6^{3-/4-}$ redox probe was measured over the typical potential range of –0.6 V to +1.0 V which overlaps with the onset of previously discussed inherent oxidation peak of GeS. This enables us to study possible interference with electrochemical responses of the redox probe and provide important insights for sensing applications. Figure 7B shows the voltammograms of $Fe(CN)_6^{3-/4-}$ on bare GC electrode, GaSe and GeS. Both bare GC and GaSe displayed a pair of reversible redox peaks with similar peak separation from ca. +0.1 V to +0.3 V and k^0_{obs} were calculated to be 1.3 × 10^{-3} cm s^{-1} (ΔE = 190 mV) and 1.1 × 10^{-3} cm s^{-1} (ΔE = 199 mV) respectively. The peak heights of the respective redox pairs are observed to be approximately equivalent. In contrast, the voltammogram for the reaction occurring on GeS is asymmetrical about the equilibrium potential, with much higher anodic current and decreased reversibility of the reaction. The poorer HET kinetics on GeS yielded k^0_{obs} of 1.5 × 10^{-5} cm s^{-1} (ΔE =

533 mV) which is two orders of magnitude lower than those of bare GC and GaSe. The much higher anodic current attained for GeS results from its own inherent oxidation peak, the onset of which overlapped with the $Fe(CN)_6^{3-/4-}$ anodic peak, resulting in interference of the electrochemical response.

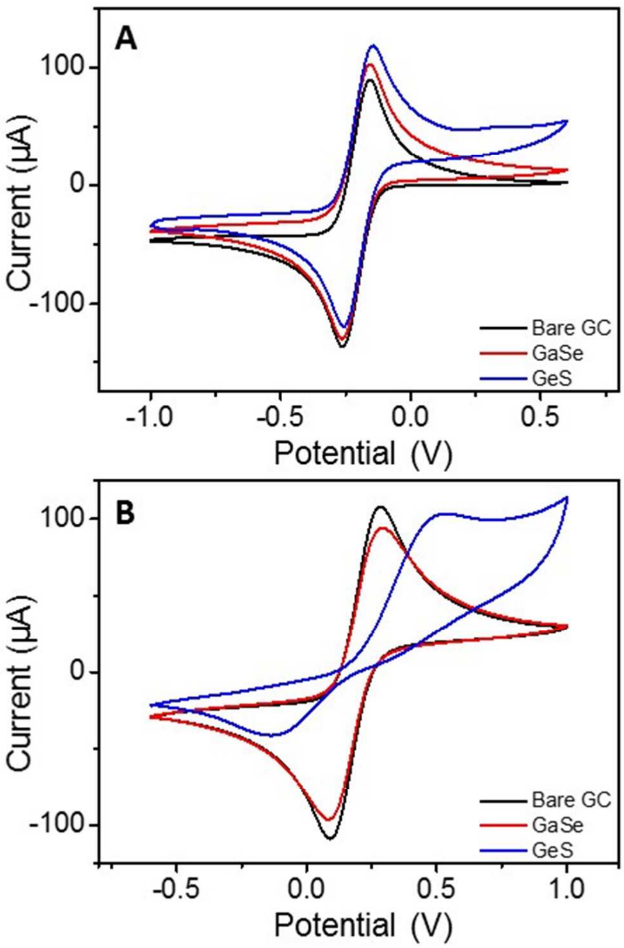

Figure 7. Cyclic voltammograms of (**A**) $Ru(NH_3)_6^{3+/2+}$ and (**B**) $Fe(CN)_6^{3-/4-}$ redox probes on bare glassy carbon (GC), GaSe and GeS. Conditions: scan rate of 100 mV s^{-1}, 50 mM PBS (pH 7.2) as supporting electrolyte.

The examinations of the electrochemical performances of $Fe(CN)_6^{3-/4-}$ and $Ru(NH_3)_6^{3+/2+}$ redox probes on GaSe and GeS ascertains the importance of investigating the inherent electroactivity of the electrode material prior to its application in sensing to establish the operational potential window. Care should be taken to prevent confusion between the inherent peak and the analyte response.

Energy-related electrochemical reactions

In the pursuit of clean energy technology, platinum catalyst has been established as the best-performing electrocatalyst for hydrogen and oxygen reduction reactions. However, its exorbitant cost and scarcity limited the proliferation of its industrial use, and spurred the quest to seek an inexpensive electrocatalyst that can surpass the platinum catalyst. The search for non-noble metal-based electrocatalysts for electrochemical production of alternative energy have been directed to a diverse range of materials, including carbon-,[63] transition metal layered double hydroxide,[64] and hybrid TMD and graphene-based catalysts.[65] These literatures are concerned with the three energy-related electrochemical reactions: oxygen reduction reaction (ORR), oxygen evolution reaction (OER) and hydrogen evolution reaction (HER). The first reaction is of paramount importance to the operation of alkaline fuel cells[66] while the last two result from the decomposition of water for energy storage purposes.[67,68] In light of the imminent energy crunch and the exigency to shift away from a hydrocarbon economy, it is therefore imperative to develop electrocatalysts capable of catalyzing these three reactions.

Bulk layered materials and their nanostructured counterparts have been understood to exhibit significantly different properties e.g. photoluminescence and lack thereof for exfoliated and bulk MoS_2 respectively.[69] It has been shown that controlled creation of surface defects on bulk crystal towards defects similar to nanostructured semiconducting MoS_2 has resulted in simultaneous decrease in photoactivity and improvement in HER catalytic activity due to increase in edge sites.[70] However, Kim et al. demonstrated enhancement in photocatalytic properties of $AgGa_{0.9}In_{0.1}S_2$ with increased exposure of nanostructured surface edges.[71] This was attributed to the unshielded incident photon which favored the migration of photogenerated electrons to the nanostructured edge. Thus, it can be observed that amongst semiconducting materials with different elemental compositions, bulk and nanostructured equivalents exhibit varying trends in their catalytic properties.

On this note, it is important to review current literature on bulk and nanostructured IIIA-VIA and IVA-VIA layered materials. Many studies have explored the synthesis of single crystals[16,17] and nanostructured[7,8,19] IIIA-VIA and IVA-VIA materials (e.g. nanosheets, nanowires, nanobelts, quantum dots etc.). However, few have targeted the electrocatalytic properties of these structures towards energy-related electrochemical reactions. Instead, much focus was placed on their photocatalytic activities that result from their semiconducting nature. Hence, it is of great interest to discuss the synthesis of GaS nanosheets by Coleman and co-workers who utilized liquid exfoliation of layered GaS powder to fabricate sheets of lateral sizes from 50–1000 nm.[25] Correlations between lateral size and HER catalytic activity indicated that smaller nanosheets exhibit better HER activity, in line with studies that report edges as active sites on materials with X-M-M-X structures.[35] Oh et al. fabricated particulate GaSe as lithium ion battery (LIB) anode material which possessed excellent cyclic stability and high discharge capacity of 760 mA h g^{-1} upon the 50th cycle.[20] This was attributed to the alloying/dealloying cycling of Li_xGa enabled by the layered GaSe. Another paper investigated the properties of nanostructured single-walled carbon nanotube–GaS_x (x = 1.2) as LIB anode material and obtained stable capacity of 575 mA g^{-1} at the 100th cycle.[28]

A perusal of current literature on related materials revealed several systems that have been investigated with regards to their photocatalytic activities. Using solid-state reactions, Domen et al. fabricated Cu-Ga-S/Se materials which were studied for their photoelectrochemical HER activities.[72,73] Under visible light irradiation and in the presence of sacrificial electron donors, both Cu-Ga-S and Cu-Ga-Se materials were shown to be catalytic towards HER and enhancement of their activities were achieved through loading of noble and base sulfide cocatalysts. Similarly, Ag-Ga-S, synthesized by solid-state reaction, exhibited hydrogen evolution rate of 296 μmol h^{-1} in visible light, which was promoted to 432 μmol h^{-1} in p–

n diode photocatalyst CdS/Ag-Ga-S.[74] The stannite-type complex sulfide, Cu-Zn-Ge-S, exhibited an evolution rate of 50 μmol h^{-1} after deposition with Ru cocatalyst.[75] The multitude of existing studies on such complex selenide and sulfide photocatalysts leaves much to be explored for simple IIIA-VIA and IVA-VIA layered systems. As a step towards bridging the gap, we embarked on the exploration of GaSe and GeS as possible electrocatalysts towards ORR, OER and HER, using linear sweep voltammetry (LSV) as a suitable electrochemical technique for such investigations.

We first examined the electrocatalytic capabilities of GaSe and GeS towards ORR, and the voltammograms obtained for these layered materials, together with those for bare GC electrode and platinum on carbon, were plotted in Figure 8A. Their respective responses in nitrogen-purged solutions are represented as dotted curves in Figure 8A as well. Pt/C exhibits the largest peak current, followed by bare GC and GaSe, while GeS shows the lowest current. The onset potential of ORR is frequently employed as a comparison parameter of the electrocatalytic activities of various materials. As anticipated, Pt/C displays the lowest onset potential at –243 mV (vs. Ag/AgCl), while the bare GC electrode demonstrates an onset potential of –295 mV. When compared against bare GC, GaSe presents a larger anodic shift of 23 mV for the onset potential. Along with its higher peak current, GaSe reveals higher electrocatalytic activity towards ORR than GeS. This may be due to its higher surface energy, as the DFT calculations demonstrated, resulting in more favorable adsorption of dissolved oxygen. While the performances of GaSe and GeS cannot rival those of electrocatalytic nanoarchitectures,[76,77] these results provided fresh insight into the electrochemical properties of these IIIA-VIA and IVA-VIA layered materials which is invaluable towards their electrocatalysis applications.

Following ORR, we moved on to evaluate the electrocatalytic performances of GaSe and GeS towards OER for the production of oxygen from water decomposition. Figure 8B examines the linear sweep voltammograms of GaSe and GeS, compared with that of the bare GC electrode. The mechanism of OER demands a highly choreographed extraction of four electrons and four protons per molecule of oxygen.[78] This translates to low activities of non-catalytic materials. From Figure 8B, it is observed that all three materials exhibit similar performances, with high onset potentials of ca. 2.2 V (vs. RHE) and low current densities. These findings suggest that GaSe and GeS show minimal electrocatalysis towards OER. A possible reason may be unfavorable free energies of OOH* and OH* intermediates on GaSe and GeS or weak stability of the surface of the materials at high anodic potentials.[79] Investigative theoretical studies will have to be performed in this regard for further elucidation.

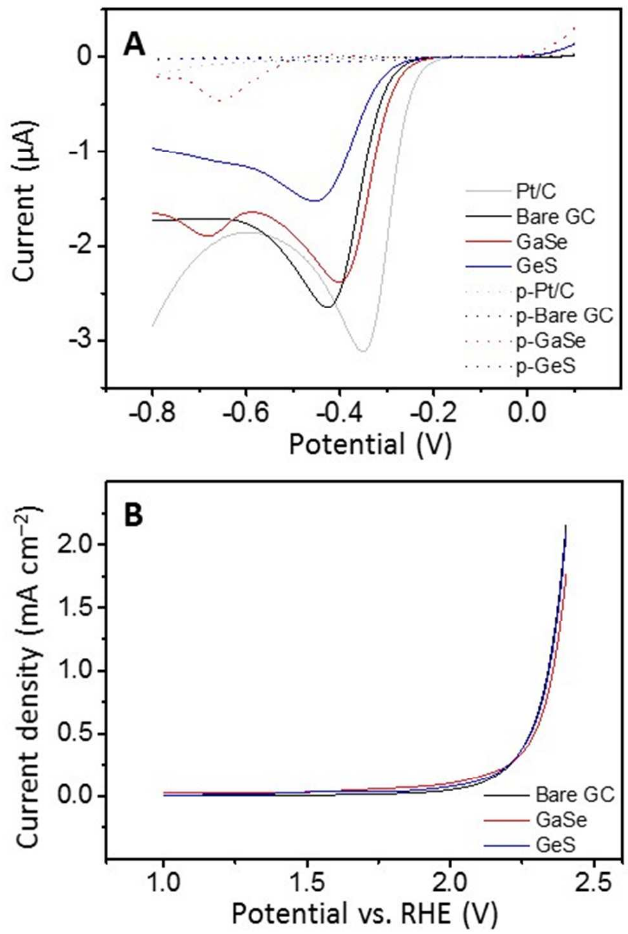

Figure 8. (**A**) Linear sweep voltammograms of oxygen reduction reaction on Pt/C, bare GC electrode, GaSe and GeS, in (solid line) oxygen- and (dotted line) nitrogen-saturated solutions. (**B**) Linear sweep voltammograms of oxygen evolution reaction on bare GC electrode, GaSe and GeS. Conditions: scan rate of (**A**) 5 mV s^{-1} and (**B**) 2 mV s^{-1}, 0.1 M KOH as supporting electrolyte.

With the recent interest in IIIA-VIA layered materials for HER application, it is timely to study the electrocatalytic performances of GaSe and GeS.[25] Furthermore, an earlier study reported electrochemical tuning of the HER catalytic activity of layered MoS_2,[80] hence it is relevant to inspect electrochemically oxidized and reduced GaSe and GeS as well. The electrochemical pre-treatment performed here is consistent with that conducted for the XPS analyses. The HER performances of Pt/C, bare GC electrode, untreated and electrochemically pre-treated GaSe and GeS are plotted in Figure 9A, while the respective Tafel slopes are presented in Figure 9B. No conducting binder was utilized as repeated HER measurements on both GaSe and GeS show current signals that exhibit minimal variations (Figure S4 in ESI). It is unsurprising that Pt/C exhibits the lowest overpotential as well as the lowest Tafel slope. On the other hand, all the examined GaSe and GeS materials demonstrate higher overpotential and Tafel slopes than the bare GC electrode whose Tafel slope of 124 mV dec^{-1} is close to the theoretical value of 120 mV dec^{-1} of the Volmer adsorption of protons, indicating that the Volmer step is the rate-limiting reaction. In contrast, the GaS nanosheets of lateral size 180 nm prepared by Coleman et al., exhibited Tafel slope of 85 mV dec^{-1} and current density of 22 mA cm^{-2} at 0.6 V.[25]

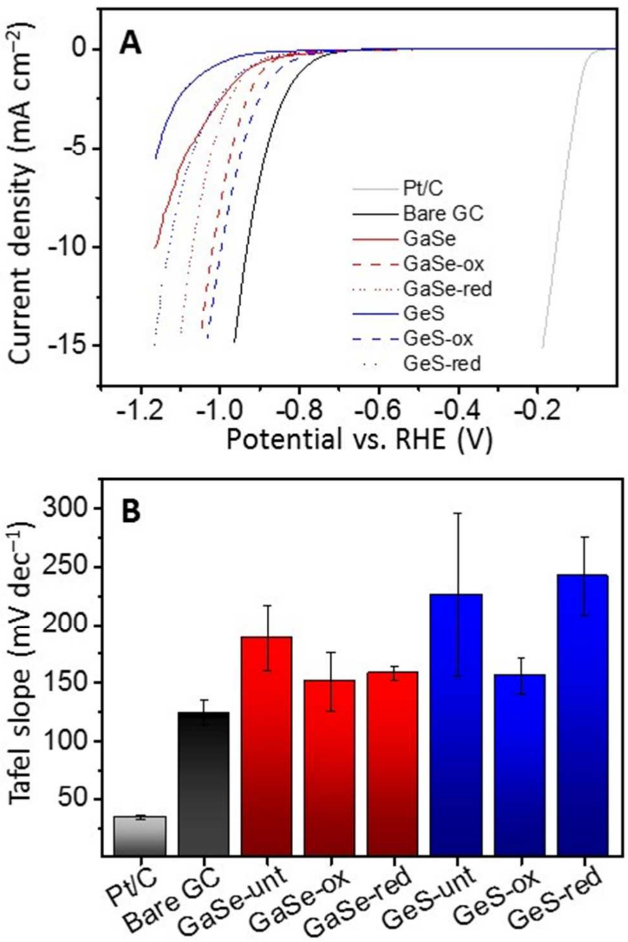

Figure 9. (**A**) Linear sweep voltammograms of hydrogen evolution reaction on Pt/C, bare GC electrode, GaSe and GeS. Conditions: scan rate of 2 mV s^{-1}, 0.5 M H_2SO_4 as supporting electrolyte. (**B**) Tafel slope values derived from the voltammograms in (**A**). Error bars indicate triplicate measurements.

An interesting observation was that unlike the MoS_2 study, where electrochemical pre-treatment enhances or impedes HER catalysis when performed at potentials of opposite polarity, both electrochemically pre-treated GaSe and GeS present lower overpotentials and Tafel slopes with improved reproducibility. Here, we attempt to elucidate the reasons for this phenomenon. From the XPS data analysis (Table 1), we observe lower atomic percentage of Ga_2O_3 on both reduced and oxidized GaSe compared to the untreated equivalent, with the reduced GaSe exhibiting a M:X ratio closer to unity. An examination of Tafel slopes of the GaSe materials reveals that the reduced GaSe displays the lowest and most stable Tafel slope, upon consideration of the error bars. This may be attributed to the removal of the passivating Ga_2O_3 which encased the GaSe active sites, leading to higher catalytic activity towards HER. Similarly, partial removal of the oxide layer for the oxidized GaSe resulted in improved Tafel slope, albeit with lower reproducibility compared to the reduced counterpart. For GeS, both reduced and oxidized materials resulted in lower Ge content due to the removal and dissolution of GeO_2, as described earlier. As such, the GeO_2 content decreases from the untreated GeS to the reduced counterpart, followed by the oxidized one. This coincides with the trend observed for Tafel slope and overpotential, whereby lower percentage of GeO_2 present on the surface of the material led to improved catalytic performance. Therefore, similar to GaSe, the oxide layer on GeS impedes its HER catalysis. These variations in electrocatalytic properties of these materials suggest the influence of changing surface sites which is related to their inherent electroactivity, substantiating the importance of fundamental studies of such layered materials.

Conclusion

We have fabricated and thoroughly characterized representative IIIA-VIA and IVA-VIA materials, GaSe and GeS, as well as conducted an in-depth investigative study on their electrochemical properties. GaSe and GeS were found to possess inherent electroactivities, with the latter exhibiting a smaller operating potential window which limits its application for electrochemical sensing towards common redox probes. Further examinations into their electrocatalytic performances toward ORR, OER and HER revealed diverging catalysis towards the different reactions. In general, GaSe exhibits enhanced catalysis compared to GeS towards ORR and HER, though both materials performed equally poor towards OER. In addition, it was established that the electrochemical pre-treatment of GaSe and GeS has successfully boosted the HER catalytic activities of both materials through removal of the encompassing surface oxide layers. These findings provide essential fundamental insight into the electrochemical properties of these IIIA-VIA and IVA-VIA layered structures. Careful characterizations of these materials prior to any electrochemical applications and appropriate utilization of these knowledge are crucial to achieve accurate and useful outcomes.

Experimental

Materials

Germanium (99.999%), gallium (99.999%), selenium (99.999%) and sulfur (99.999%) were purchased from STREM, USA. Quartz glass ampoules of the size 120 × 30 mm (wall thickness 1.5–2 mm) were made from high purity quart tubes (Heraeus Quartzglass, Germany). Hydrofluoric acid and acetone were obtained from Penta, Czech Republic. *N*,*N*-dimethylformamide, sulfuric acid, potassium hydroxide, potassium phosphate dibasic, sodium phosphate monobasic, sodium chloride, potassium chloride, potassium hexacyanoferrate(III), potassium hexacyanoferrate(II) trihydrate, and hexaammineruthenium(III) chloride were purchased from Sigma-Aldrich. Glassy carbon (GC) electrodes, Ag/AgCl reference electrode and platinum electrode were obtained from CH Instruments. Milli-Q water with a resistivity of 18.2 MΩ cm was utilized throughout for the preparation of electrolytes.

Apparatus and Methods

Scanning electron microscopy (SEM) and energy-dispersive X-ray spectroscopy (EDS) were performed with a JEOL 7600F field-emission SEM (JEOL, Japan), at an acceleration voltage of 5 kV and 20 kV respectively. 1 µL of 0.2 mg mL^{-1} and 1 mg mL^{-1} of the materials were dropcasted on a silicon wafer for SEM and EDS purposes correspondingly. Raman spectroscopy was executed with a confocal micro-Raman LabRam HR instrument from Horiba Scientific in backscattering geometry with a CCD detector, a 100× objective appended to an Olympus optical microscope, as well as a 514.5 nm Ar laser. Prior to measurements, calibration was performed by employing an internal silicon reference at 520 cm^{-1} to obtain a peak position resolution of less than 1 cm^{-1}. XPS was carried out by utilizing a conventional nonmonochromated X-ray source using the Mg Kα line (SPECS XR50, $h\nu$ = 1253 eV, 200 W) and a multichannel energy analyzer (SPECS Phoibos 100 MCD-5). Wide-scan and high-resolution Ga 3*d*, Se 3*d*, Ge 3*s* and S 2*p* core-level spectra were collected. Relative sensitivity factors were used for the evaluation of metal-to-chalcogen ratios. Electrochemical measurements using the cyclic voltammetry (CV) and linear sweep voltammetry (LSV) techniques, and electrochemical activation by chronoamperometry were performed with a μAutolab type III electrochemical analyzer (Eco Chemie, The Netherlands) operated using the software NOVA 1.8 (Eco Chemie) and General Purpose Electrochemical Systems Version 4.9 software (Eco Chemie) respectively. X-ray powder diffraction data were collected at room temperature with an Bruker D8 Discoverer powder diffractometer with parafocusing Bragg-Brentano geometry using CuKα radiation (λ = 0.15418 nm, U = 40 kV, I = 40 mA). Data were scanned with an ultrafast detector X'Celerator over the angular range 5–80° (2θ) with a step size of 0.019° (2θ). Data evaluation was performed in the software package HighScore Plus 3.0e.

Procedures

Synthesis of GaSe

Quartz glass ampoules were thoroughly washed with hydrofluoric acid, deionized water and acetone prior to usage. The ampoules were then heated by an oxygen-hydrogen torch under high vacuum (< 5 × 10^{-3} Pa) to remove any impurities. A stoichiometric mixture of granulated gallium and selenium (15 g) was put in a quartz glass ampoule (25 mm × 150 mm) and subsequently evacuated (< 5 × 10^{-3} Pa) using a diffusion pump. The evacuated ampoule was then secured using an oxygen-hydrogen torch, after which the reaction mixture was heated to 970 °C at 1 °C min^{-1}. The reaction mixture was then cooled after 1 h at 970 °C, with a cooling rate of 1 °C min^{-1}. For electrochemical characterizations, the prepared crystals were pulverized in agate mortar for 30 min. The obtained crystals are shown in Supporting Information (Figure S5 in ESI). The synthesis procedure is based on the knowledge of Ga-Se phase diagram since the GaSe melt congruently at 960 °C.[81]

Synthesis of GeS

Quartz glass ampoules were thoroughly cleaned with hydrofluoric acid, deionized water and acetone before fabrication. Thereafter, the ampoules were heated by an oxygen-hydrogen torch under high vacuum (< 5 × 10^{-3} Pa) to remove any impurities. A stoichiometric mixture of granulated germanium and sulfur (10 g) was placed in a quartz glass ampoule (25 mm × 150 mm) and then evacuated to below 5 × 10^{-3} Pa using a diffusion pump. The evacuated ampoule was subsequently sealed using an oxygen-hydrogen torch. Subsequently, the reaction mixture was heated to 700 °C at 1 °C min^{-1}. After 5 h of heating, the reaction mixture was cooled at 1 °C min^{-1}. For electrochemical characterizations, the prepared crystals were pulverized in agate mortar for 30 min. The obtained crystals are shown in Supporting Information (Figure S5 in ESI). The synthesis procedure is based on the knowledge of Ge-S phase diagram since the GeS melt congruently at 667 °C.[82]

Electronic structure calculations

The band structures and total energies of GeS (Pnma, V_c = 163 Å3, z = 4) and GaSe (P-6m2, V_c = 0.195 nm^3, z = 4) in a bulk form and as a single layer were calculated within density functional theory (DFT) using APW+lo basis set and generalized gradient approximation (GGA, PBE96 parametrization scheme)[83] for exchange correlation potential as implemented in the Wien2k software package.[84] The plane wave cut-off energy of 230 eV and the tetrahedron method with the respective k-meshes 13×11×4, 13×11×1 for the bulk and monolayer of GeS and 12×12×4 and 12×12×1 for GaSe were used. The two-dimensional character of the monolayer was simulated by introducing a 15 Å thick vacuum in the corresponding direction. All calculations were performed as non-spin polarized.

Electrochemical procedures

GaSe and GeS (5.0 mg mL^{-1}) were individually prepared in *N*,*N*-dimethylformamide (DMF), and subsequently ultrasonicated for 1 h to achieve well-dispersed suspensions. Before every measurement, the glassy carbon (GC) electrode surface was renewed to a mirror finish by polishing with 0.05 μm alumina particles on a polishing pad, followed by rinsing with deionized water and then thoroughly dried. After 5 min of sonication, 1 μL aliquot of the materials suspension was drop-casted onto the GC electrode surface using a micropipette. To obtain randomly distributed material on the GC surface, the DMF solvent was allowed to evaporate at room temperature. No conducting binder was used as multiple HER measurements conducted on both GaSe- and GeS-modified GC electrodes show current signals that exhibit minimal variations (Figure S4 in ESI). A coating of the material remain visible on the GC surface even after the measurements, indicating that minimal material has dislodged from the surface (Figure S4, insets). Cyclic voltammetry (CV) and linear sweep voltammetry (LSV) measurements were conducted in a 5 mL electrochemical cell at room temperature using a three-electrode configuration, with the modified GC, Ag/AgCl and Pt electrodes as the working, reference and counter electrodes respectively. Phosphate buffer solution (PBS, 50 mM, pH 7.2) was utilized as the supporting electrolyte for the inherent electrochemistry studies, and $Fe(CN)_6^{3-/4-}$ and $Ru(NH_3)_6^{3+/2+}$ redox probes measurements, while sulfuric acid (0.5 M) was employed for the hydrogen evolution reaction (HER) investigations. Potassium hydroxide (0.1 M) was used as the supporting electrolyte for both oxygen evolution and reduction reactions (OER and ORR respectively). Electrochemical oxidative and reductive pre-treatments of the crystals were conducted through chronoamperometry in PBS at +1.5 V and –1.5 V respectively, for 10 min prior to measurements. All CV measurements were executed at a scan rate of 100 mV s^{-1}, and LSV scans at 2 mV s^{-1} for OER and 5 mV s^{-1} for ORR. Triplicate measurements were performed for all electrochemical examinations. The onset potential of ORR measurements is defined as the potential at which 10% of peak current is achieved. All potentials are relative to Ag/AgCl unless otherwise indicated, and all solutions were purged with nitrogen gas, unless otherwise stated.

Calculations of HET rate constants

For $Fe(CN)_6^{3-/4-}$ and $Ru(NH_3)_6^{3+/2+}$, the HET rate constants (k^0) were assessed using the Nicholson method,[61] whereby the peak-to-peak separation (ΔE) of the electrochemical process is correlated to a dimensionless parameter ψ and, in turn, to k^0. The roughness factor was not taken into consideration. The diffusion coefficients of the oxidized (O) and reduced (R) configurations of the redox probes used for the calculations were $D_O = D_R = 7.26 \times 10^{-6}$ cm^2 s^{-1} ($Fe(CN)_6^{3-/4-}$), and $D_O = D_R = 9.1 \times 10^{-6}$ cm^2 s^{-1} ($Ru(NH_3)_6^{3+/2+}$), in 0.1 M KCl.[85,86]

ASSOCIATED CONTENT

SUPPORTING INFORMATION

EDS mappings and elemental spectra, X-ray diffraction patterns, photoluminescence spectra, and LSVs of repeated HER. This information is available free of charge via the Internet at http://pubs.acs.org/.

AUTHOR INFORMATION

Corresponding Author

* Email: pumera@ntu.edu.sg

Author Contributions

‡These authors contributed equally.

Funding Sources

M. P. thanks to Tier 2 fund (13/99). Z.S. and D.S. were supported by Czech Science Foundation (GACR No. 15-07912S).

Notes

The authors declare no competing financial interest.

REFERENCES

(1) Wang, Q.; Kang, S.-Z.; Li, X.; Yang, Y.-W.; Qin, L.; Mu, J., A Facile Preparation of Crystalline GeS_2 Nanoplates and their Photocatalytic Activity. *J. Alloys Compd.* **2015,** 631, 21-25.
(2) Feng, K.; Mei, D.; Bai, L.; Lin, Z.; Yao, J.; Wu, Y., Synthesis, Structure, Physical Properties, and Electronic Structure of $KGaSe_2$. *Solid State Sci.* **2012,** 14, 1152-1156.
(3) Zhang, S.-R.; Zhu, S.-F.; Zhao, B.-J.; Xie, L.-H.; Song, K.-H., First-Principles Study of the Elastic, Electronic and Optical Properties of ε-GaSe Layered Semiconductor. *Physica B* **2014,** 436, 188-192.
(4) Hashimzade, F. M.; Huseinova, D. A.; Jahangirli, Z. A.; Mehdiyev, B. H., Second-Order Phase Transition at High-Pressure in GeS Crystal. *Physica B* **2014,** 454, 56-59.
(5) Tan, S. M.; Ambrosi, A.; Sofer, Z.; Huber, Š.; Sedmidubský, D.; Pumera, M., Pristine Basal- and Edge-Plane-Oriented Molybdenite MoS_2 Exhibiting Highly Anisotropic Properties. *Chem. Eur. J.* **2015,** 21, 7170-7178.
(6) Wang, L.; Sofer, Z.; Pumera, M., Voltammetry of Layered Black Phosphorus: Electrochemistry of Multilayer Phosphorene. *ChemElectroChem* **2015,** 2, 324-327.
(7) Peng, H.; Meister, S.; Chan, C. K.; Zhang, X. F.; Cui, Y., Morphology Control of Layer-Structured Gallium Selenide Nanowires. *Nano Lett.* **2007,** 7, 199-203.
(8) Li, C.; Huang, L.; Snigdha, G. P.; Yu, Y.; Cao, L., Role of Boundary Layer Diffusion in Vapor Deposition Growth of Chalcogenide Nanosheets: The Case of GeS. *ACS Nano* **2012,** 6, 8868-8877.
(9) Mayorga-Martinez, C. C.; Sofer, Z.; Pumera, M., Layered Black Phosphorus as a Selective Vapor Sensor. *Angew. Chem. Int. Ed.* **2015**, 54, 14317-14320.
(10) Favron, A.; Gaufrès, E.; Fossard, F.; Phaneuf-L'Heureux, A.-L.; Tang, N. Y.-W.; Lévesque, P. L.; Loiseau, A.; Leonelli, R.; Francoeur, S.; Martel, R., Photooxidation and Quantum Confinement Effects in Exfoliated Black Phosphorus. *Nat. Mater.* **2015**, 14, 826-833.
(11) a) Latiff, N. M.; Teo, W. Z.; Sofer, Z.; Fisher, A. C.; Pumera, M., The Cytotoxicity of Layered Black Phosphorus. *Chem. Eur. J.* **2015**, 21, 13991-13995. b) Latiff, N.; Teo, W. Z.; Sofer, Z; Huber, S; Fisher, A. C.; *RSC Adv.* 2015, 5, 67485.
(12) and Martin Pumera
(13) Zakery, A.; Elliott, S. R., *Optical Nonlinearities in Chalcogenide Glasses and their Applications*. Springer-Verlag: Heidelberg, Germany, 2007; Vol. 135, p 10-13.
(14) Shen, G.; Chen, D.; Chen, P.-C.; Zhou, C., Vapor-Solid Growth of One-Dimensional Layer-Structured Gallium Sulfide Nanostructures. *ACS Nano* **2009,** 3, 1115-1120.
(15) Singh, N. B.; Suhre, D. R.; Balakrishna, V.; Marable, M.; Meyer, R., Far-Infrared Conversion Materials: Gallium Selenide for Far-Infrared Conversion Applications. *Prog. Cryst. Growth Charact. Mater.* **1998,** 37, 47-102.
(16) Borshchevsky, A., *Preparation of Thermoelectric Materials from Melts*. CRC Press: Florida, U.S.A., 1995; Vol.1, p 90.
(17) Voevodin, V. G.; Voevodina, O. V.; Bereznaya, S. A.; Korotchenko, Z. V.; Morozov, A. N.; Sarkisov, S. Y.; Fernelius, N. C.; Goldstein, J. T., Large Single Crystals of Gallium Selenide: Growing, Doping by In and Characterization. *Opt. Mater.* **2004,** 26, 495-499.
(18) Ni, Y.; Wu, H.; Huang, C.; Mao, M.; Wang, Z.; Cheng, X., Growth and Quality of Gallium Selenide (GaSe) Crystals. *J. Cryst. Growth* **2013**, 381, 10-14.
(19) Adriaenssens, G. J.; Gheorghiu, A.; Sénémaud, C.; Qamhieh, N.; Bollé, N.; Sleeckx, E.; Nagels, P., Comparison between Electrical Properties and Electronic Structure of Variously-Prepared Germanium Selenide Films. *J. Non-Cryst. Solids* **1996,** 198-200, 675-679.
(20) Gujar, T. P.; Shinde, V. R.; Park, J.-W.; Lee, H. K.; Jung, K.-D.; Joo, O.-S., Electrodeposition of Photoactive 1D Gallium Selenide Quantum Dots. *Electrochim. Acta* **2008,** 54, 829-834.
(21) Jeong, J.-H.; Jung, D.-W.; Oh, E.-S., Lithium Storage Characteristics of a New Promising Gallium Selenide Anodic Material. *J. Alloys Compd.* **2014,** 613, 42-45.
(22) Gedi, S.; Reddy, V. R. M.; Park, C.; Chan-Wook, J.; Reddy, R. K. T., Comprehensive optical studies on SnS layers synthesized by chemical bath deposition. *Opt. Mater.* **2015,** 42, 468-475.
(23) Li, H.; Ji, J.; Zheng, X.; Ma, Y.; Jin, Z.; Ji, H., Preparation of SnS quantum dots for solar cells application by an *in-situ* solution chemical reaction process. *Mater. Sci. Semicond. Process.* **2015,** 36, 65-70.
(24) Srivastava, A.; Chandiramouli, R., Band Structure and Transport Studies on Impurity Substituted InSe Nanosheet – a First-Principles Investigation. *Superlattice Microst.* **2015,** 79, 135-147.
(25) Kunjomana, A. G.; Chandrasekharan, K. A.; Teena, M., Physical Properties of Vapour Grown Indium Monotelluride Platelets. *J. Cryst. Growth* **2015,** 411, 81-87.
(26) Harvey, A.; Backes, C.; Gholamvand, Z.; Hanlon, D.; McAteer, D.; Nerl, H. C.; McGuire, E.; Seral-Ascaso, A.; Ramasse, Q. M.; McEvoy, N.; Winters, S.; Berner, N. C.; McCloskey, D.; Donegan, J. F.; Duesberg, G. S.; Nicolosi, V.; Coleman, J. N., Preparation of Gallium Sulfide Nanosheets by Liquid Exfoliation and Their Application as Hydrogen Evolution Catalysts. *Chem. Mater.* **2015,** 27, 3483-3493.
(27) Jariwala, D.; Sangwan, V. K.; Lauhon, L. J.; Marks, T. J.; Hersam, M. C., Emerging Device Applications for Semiconducting Two-Dimensional Transition Metal Dichalcogenides. *ACS Nano* **2014,** 8, 1102-1120.
(28) Ariga, K.; Yamauchi, Y.; Rydzek, G.; Ji, Q.; Yonamine, Y.; Wu, K. C.-W.; Hill, J. P., Layer-by-layer Nanoarchitectonics:

Invention, Innovation, and Evolution. *Chem. Lett.* **2014,** 43, 36-68.
(29) Meng, X.; He, K.; Su, D.; Zhang, X.; Sun, C.; Ren, Y.; Wang, H.-H.; Weng, W.; Trahey, L.; Canlas, C. P.; Elam, J. W., Gallium Sulfide–Single-Walled Carbon Nanotube Composites: High-Performance Anodes for Lithium-Ion Batteries. *Adv. Funct. Mater.* **2014,** 24, 5435-5442.
(30) Ma, Y.; Dai, Y.; Guo, M.; Yu, L.; Huang, B., Tunable Electronic and Dielectric Behavior of GaS and GaSe Monolayers. *Phys. Chem. Chem. Phys.* **2013,** 15, 7098-7105.
(31) Zhu, Z.; Cheng, Y.; Schwingenschlögl, U., Topological Phase Transition in Layered GaS and GaSe. *Phys. Rev. Lett.* **2012,** 108, 266805.
(32) Errandonea, D.; Segura, A.; Manjón, F. J.; Chevy, A.; Machado, E.; Tobias, G.; Ordejón, P.; Canadell, E., Crystal Symmetry and Pressure Effects on the Valence Band Structure of γ-InSe and ε-GaSe: Transport Measurements and Eectronic Structure Calculations. *Phys. Rev. B* **2005,** 71, 125206.
(33) O'Hare, P. A. G.; Curtiss, L. A., Thermochemistry of (Germanium+Sulfur) IV. Critical Evaluation of the Thermodynamic Properties of Solid and Gaseous Germanium(II) Sulfide GeS and Germanium(IV) Disulfide GeS_2, and Digermanium Disulfide Ge_2S_2(g). Enthalpies of Dissociation of Bonds in GeS(g), GeS_2(g), and Ge_2S_2(g). *J. Chem. Thermodynamics* **1995**, 27, 643-662.
(34) Hahn, H.; Burow, F., Über die Bildungsenthalpien der Sulfide, Selenide und Telluride des Galliums und Indiums. *Angew. Chem.* **1956**, 68, 382.
(35) Zavrazhnov, A.Y., PTx Phase Diagrams of Gallium Chalcogenides Studied Using an Additional Component. *Russ. J. Inorg. Chem.* **2003**, 48, 1577-1590.
(36) Gerischer, H.; Gobrecht, J., The Photoelectrochemistry of Gallium Selenide. *Ber. Bunsenges Phys. Chem.* **1980,** 84, 596-601.
(37) Tyagai, V. A.; Bondarenko, V. N.; Krasiko, A. N.; Bletskan, D. I.; Sheka, V. I., Electroreflection Spectra of Germanium and Tin Monochalcogenides. *Fiz. Tverd. Tela* **1976**, 18, 1433-1436.
(38) Wieting, T. J.; Verble, J. L., Interlayer Bonding and the Lattice Vibrations of *β*-GaSe. *Phys. Rev. B* **1972,** 5, 1473-1479.
(39) Gasanly, N. M.; Aydinli, A.; Özkan, H.; Kocabaş, C., Temperature-Dependent Raman Scattering Spectra of ε-GaSe Layered Crystal. *Mater. Res. Bull.* **2002,** 37, 169-176.
(40) Wiley, J. D.; Buckel, W. J.; Schmidt, R. L., Infrared Reflectivity and Raman Scattering in GeS. *Phys. Rev. B* **1976,** 13, 2489-2496.
(41) Mateleshko, N.; Mitsa, V.; Holomb, R., Structural Studies of Technologically Modificated GeS_2 Glasses and Film. *Physica B* **2004,** 349, 30-34.
(42) Takebe, H.; Maeda, H.; Morinaga, K., Compositional Variation in the Structure of Ge-S Glasses. *J. Non-Cryst. Solids* **2001,** 291, 14-24.
(43) Barr, T. L.; Seal, S., Nature of the Use of Adventitious Carbon as a Binding Energy Standard. *J. Vac. Sci. Technol.* **1995,** 13, 1239-1246.
(44) Iwakuro, H.; Tatsuyama, C.; Ichimura, S., XPS and AES Studies on the Oxidation of Layered Semiconductor GaSe. *Jpn. J. Appl. Phys.* **1982,** 21, 94-99.
(45) Murugesan, S.; Kearns, P.; Stevenson, K. J., Electrochemical Deposition of Germanium Sulfide from Room-Temperature Ionic Liquids and Subsequent Ag Doping in an Aqueous Solution. *Langmuir* **2012,** 28, 5513-5517.
(46) Tabet, N.; Faiz, M.; Hamdan, N. M.; Hussain, Z., High Resolution XPS Study of Oxide Layers Grown on Ge Substrates. *Surf. Sci.* **2003,** 523, 68-72.
(47) Ghazali, N. M.; Mahmood, M. R.; Yasui, K.; Hashim, A. M., Electrochemically Deposited Gallium Oxide Nanostructures on Silicon Substrates. *Nanoscale Res. Lett.* **2014,** 9, 120.
(48) Matovu, J. B.; Ong, P.; Leunissen, L. H. A.; Krishnan, S.; Babu, S. V., Fundamental Investigation of Chemical Mechanical Polishing of GaAs in Silica Dispersions: Material Removal and Arsenic Trihydride Formation Pathways. *ECS J. Solid State Sci. Technol.* **2013,** 2, P432-P439.
(49) Chung, Y.; Lee, C.-W., Electrochemistry of Gallium. *J. Electrochem. Sci. Technol.* **2013,** 4, 1-18.
(50) Hovis, J. S.; Hamers, R. J.; Greenlief, C. M., Preparation of Clean and Atomically Flat Germanium(001) Surfaces. *Surf. Sci.* **1999,** 440, L815-L819.
(51) Prabhakaran, K.; Ogino, T., Oxidation of Ge(100) and Ge(111) surfaces: an UPS and XPS study. *Surf. Sci.* **1995,** 325, 263-271.
(52) Mikkelsen, Ø.; Schrøder, K. H., Alloy Electrodes with High Hydrogen Overvoltage for Analytical Use in Voltammetry. Some Preliminary Results. *Analyst* **2000,** 125, 2163-2165.
(53) Nasir, M. Z. M.; Sofer, Z.; Ambrosi, A.; Pumera, M., A Limited Anodic and Cathodic Potential Window of MoS_2: Limitations in Electrochemical Applications. *Nanoscale* **2015,** 7, 3126-3129.
(54) Bonde, J.; Moses, P. G.; Jaramillo, T. F.; Nørskov, J. K.; Chorkendorff, I., Hydrogen Evolution on Nano-Particulate Transition Metal Sulfides. *Faraday Discuss.* **2008,** 140, 219-231.
(55) Wu, S.; Zeng, Z.; He, Q.; Wang, Z.; Wang, S. J.; Du, Y.; Yin, Z.; Sun, X.; Chen, W.; Zhang, H., Electrochemically Reduced Single-Layer MoS_2 Nanosheets: Characterization, Properties, and Sensing Applications. *Small* **2012,** 8, 2264-2270.
(56) Eng, A. Y. S.; Ambrosi, A.; Chua, C. K.; Šaněk, F.; Sofer, Z.; Pumera, M., Unusual Inherent Electrochemistry of Graphene Oxides Prepared Using Permanganate Oxidants. *Chem. Eur. J.* **2013,** 19, 12673-12683.
(57) Lim, C. S.; Chua, C. K.; Sofer, Z.; Klímová, K.; Boothroyd, C.; Pumera, M., Layered Transition Metal Oxyhydroxides as Tri-Functional Electrocatalysts. *J. Mater. Chem. A* **2015,** 3, 11920-11929.
(58) Chua, C. K.; Sofer, Z.; Lim, C. S.; Pumera, M., Inherent Electrochemistry of Layered Post-Transition Metal Halides: The Unexpected Effect of Potential Cycling of PbI_2. *Chem. Eur. J.* **2015,** 21, 3073-3078.
(59) Lim, C. S.; Chua, C. K.; Sofer, Z.; Jankovský, O.; Pumera, M., Alternating Misfit Layered Transition/Alkaline Earth Metal Chalcogenide $Ca_3Co_4O_9$ as a New Class of Chalcogenide Materials for Hydrogen Evolution. *Chem. Mater.* **2014,** 26, 4130-4136.
(60) Lim, C. S.; Wang, L.; Chua, C. K.; Sofer, Z.; Jankovský, O.; Pumera, M., High Temperature Superconducting Materials as Bi-Functional Catalysts for Hydrogen Evolution and Oxygen Reduction. *J. Mater. Chem. A* **2015,** 3, 8346-8352.
(61) Eng, A. Y. S.; Ambrosi, A.; Sofer, Z.; Šimek, P.; Pumera, M., Electrochemistry of Transition Metal Dichalcogenides: Strong Dependence on the Metal-to-Chalcogen Composition and Exfoliation Method. *ACS Nano* **2014,** 8, 12185-12198.
(62) Nicholson, R. S., Theory and Application of Cyclic Voltammetry for Measurement of Electrode Reaction Kinetics *Anal. Chem.* **1965,** 37, 1351-1355.
(63) McCreery, R. L., Advanced Carbon Electrode Materials for Molecular Electrochemistry. *Chem. Rev.* **2008,** 108, 2646-2687.
(64) Cheng, X.-B.; Zhang, Q.; Wang, H.-F.; Tian, G.-L.; Huang, J.-Q.; Peng, H.-J.; Zhao, M.-Q.; Wei, F., Nitrogen-Doped Herringbone Carbon Nanofibers With Large Lattice Spacings and Abundant Edges: Catalytic Growth and Their Applications in Lithium Ion Batteries and Oxygen Reduction Reactions. *Catal. Today* **2015,** 249, 244-251.
(65) Jiang, J.; Zhang, A.; Li, L.; Ai, L., Nickel–cobalt Layered Double Hydroxide Nanosheets as High-Performance Electrocatalyst for Oxygen Evolution Reaction. *J. Power Sources* **2015,** 278, 445-451.
(66) Li, Y.; Wang, H.; Xie, L.; Liang, Y.; Hong, G.; Dai, H., MoS_2 Nanoparticles Grown on Graphene: an Advanced Catalyst for the Hydrogen Evolution Reaction. *J. Am. Chem. Soc.* **2011,** 133, 7296-7299.

(67) Spendelow, J. S.; Wieckowski, A., Electrocatalysis of Oxygen Reduction and Small Alcohol Oxidation in Alkaline Media. *Phys. Chem. Chem. Phys.* **2007,** 9, 2654-2675.
(68) Walter, M. G.; Warren, E. L.; McKone, J. R.; Boettcher, S. W.; Mi, Q.; Santori, E. A.; Lewis, N. S., Solar Water Splitting Cells. *Chem. Rev.* **2010,** 110, 6446-6473.
(69) Barber, J., Photosynthetic Energy Conversion: Natural and Artificial. *Chem. Soc. Rev.* **2009,** 38, 185-196.
(70) Splendiani, A.; Sun, L.; Zhang, Y.; Li, T.; Kim, J.; Chim, C.-Y.; Galli, G.; Wang, F., Emerging Photoluminescence in Monolayer MoS_2. *Nano Lett.* **2010,** 10, 1271–1275.
(71) Chen, Z.; Forman, A. J.; Jaramillo, T. F., Bridging the Gap between Bulk and Nanostructured Photoelectrodes: The Impact of Surface States on the Electrocatalytic and Photoelectrochemical Properties of MoS_2. *J. Phys. Chem. C* **2013,** 117, 9713-9722.
(72) Jang, J. S.; Borse, P. H.; Lee, J. S.; Choi, S. H.; Kim, H. G., Indium Induced Band Gap Tailoring in $AgGa_{1-x}In_xS_2$ Chalcopyrite Structure for Visible Light Photocatalysis. *J. Chem. Phys.* **2008,** 128, 154717.
(73) Tabata, M.; Maeda, K.; Ishihara, T.; Minegishi, T.; Takata, T.; Domen, K., Photocatalytic Hydrogen Evolution from Water Using Copper Gallium Sulfide under Visible-Light Irradiation. *J. Phys. Chem. C* **2010,** 114, 11215-11220.
(74) Kumagai, H.; Minegishi, T.; Moriya, Y.; Kubota, J.; Domen, K., Photoelectrochemical Hydrogen Evolution from Water Using Copper Gallium Selenide Electrodes Prepared by a Particle Transfer Method. *J. Phys. Chem. C* **2014,** 118, 16386-16392.
(75) Jang, J. S.; Hwang, D. W.; Lee, J. S., CdS–$AgGaS_2$ Photocatalytic Diodes for Hydrogen Production from Aqueous Na_2S/Na_2SO_3 Electrolyte Solution under Visible Light ($\lambda \geq$ 420 nm). *Catal. Today* **2007,** 120, 174-181.
(76) Tsuji, I.; Shimodaira, Y.; Kato, H.; Kobayashi, H.; Kudo, A., Novel Stannite-type Complex Sulfide Photocatalysts A^{I}_2-Zn-A^{IV}-S_4 (A^{I} = Cu and Ag; A^{IV} = Sn and Ge) for Hydrogen Evolution under Visible-Light Irradiation *Chem. Mater.* **2010,** 22, 1402-1409.
(77) Liang, Y.; Li, Y.; Wang, H.; Zhou, J.; Wang, J.; Regier, T.; Dai, H., Co_3O_4 Nanocrystals on Graphene as a Synergistic Catalyst for Oxygen Reduction Reaction. *Nat. Mater.* **2011,** 10, 780-786.
(78) Duan, J.; Zheng, Y.; Chen, S.; Tang, Y.; Jaroniec, M.; Qiao, S. Z., Mesoporous Hybrid Material Composed of Mn_3O_4 Nanoparticles on Nitrogen-Doped Graphene for Highly Efficient Oxygen Reduction Reaction. *Chem. Commun.* **2013,** 49, 7705-7707.
(79) Eisenberg, R.; Gray, H. B., Preface on Making Oxygen. *Inorg. Chem.* **2008,** 47, 1697-1699.
(80) Jiao, Y.; Zheng, Y.; Jaroniec, M.; Qiao, S. Z., Design of Electrocatalysts for Oxygen- and Hydrogen-Involving Energy Conversion Reactions. *Chem. Soc. Rev.* **2015,** 44, 2060-2086.
(81) Chia, X.; Ambrosi, A.; Sedmidubský, D.; Sofer, Z.; Pumera, M., Precise Tuning of the Charge Transfer Kinetics and Catalytic Properties of MoS_2 Materials *via* Electrochemical Methods. *Chem. Eur. J.* **2014,** 20, 17426-17432.
(82) Okamoto, H., Ga-Se (Gallium-Selenium) *J. Phase Equilib. Diff.* **2009**, 30, 658.
(83) Bletskan, D. I., Phase Equilibrium in the Systems A^{IV} – B^{VI}. *J. Ovonic Res.* **2005**, 1, 53-60.
(84) Perdew, J. P.; Burke, K.; Ernzerhof, M., Generalized Gradient Approximation Made Simple. *Phys. Rev. Lett.* **1996**, 77, 3865-3868.
(85) Blaha, P.; Schwarz, K.; Madsen, G.; Kvasnicka D.; Luitz, J. *WIEN2k*, An Augmented Plane Wave+Local Orbitals Program for Calculating Crystal Properties. Karlheinz Schwarz, Techn. Universität Wien, Austria, **2001**, ISBN 3-9501031-1-2.
(86) Konopka, S. J.; McDuffie, B., Diffusion Coefficients of Ferri- and Ferrocyanide Ions in Aqueous Media, Using Twin-Electrode Thin-layer Electrochemistry. *Anal. Chem.* **1970,** 42, 1741-1746.
(87) Marken, F.; Eklund, J. C.; Compton, R. G., Voltammetry in the Presence of Ultrasound: can Ultrasound Modify Heterogeneous Electron Transfer Kinetics? *J. Electroanal. Chem.* **1995,** 395, 335-339.